Spectrochimica Acta Part A: Molecular and Biomolecular Spectroscopy 169 (2016) 87–94

Contents lists available at ScienceDirect

Spectrochimica Acta Part A: Molecular and Biomolecular Spectroscopy

journal homepage: www.elsevier.com/locate/saa

Fluorescence sensor for sequential detection of zinc and phosphate ions

Miran An [a], Bo-Yeon Kim [a], Hansol Seo [a], Aasif Helal [b,*], Hong-Seok Kim [a,*]

[a] Department of Applied Chemistry, Kyungpook National University, Daegu 41566, Republic of Korea
[b] Center of Research Excellence in Nanotechnology, King Fahd University of Petroleum and Minerals, Dhahran 31261, Saudi Arabia

ARTICLE INFO

Article history:
Received 1 November 2015
Received in revised form 28 April 2016
Accepted 17 June 2016
Available online 18 June 2016

Keywords:
Fluorogenic chemosensor
Thiazole sulfonamide
Sequential recognition
Zinc
Phosphate

ABSTRACT

A new, highly selective turn-on fluorescent chemosensor based on 2-(2′-tosylamidophenyl)thiazole (**1**) for the detection of zinc and phosphate ions in ethanol was synthesized and characterized. Sensor **1** showed a high selectivity for zinc compared to other cations and sequentially detected hydrogen pyrophosphate and hydrogen phosphate. The fluorescence mechanism can be explained by two different mechanisms: (i) the inhibition of excited-state intramolecular proton transfer (ESIPT) and (ii) chelation-induced enhanced fluorescence by binding with Zn^{2+}. The sequential detection of phosphate anions was achieved by the quenching and subsequent revival of ESIPT.

1. Introduction

Molecular fluorescent chemosensors for the recognition of cations and anions have attracted much attention for important and diverse ecological, biological, and clinical applications [1–4]. Fluorescent chemosensors have the advantages of real-time monitoring with fast response times, intrinsic high sensitivity, and ease of handling compared to other optical sensors [5,6]. The sensing of Zn^{2+} ions, the second most abundant transition metal in the human body, in an aqueous media is ecologically and biochemically relevant because they play crucial roles in biological systems. Zn^{2+} ions are vital for many cellular processes [7] such as apoptosis [8], DNA synthesis [9], neurotransmission [10,11], gene expression [12], modulation of diverse ion channels [13], and signal transduction [14]. Zn^{2+} ions are also an essential component of many enzymes, e.g., carbonic anhydrase, transcription factors, and zinc finger proteins, in which they play catalytic or structural roles [15]. Clinically, diverse Zn^{2+}-based compounds have been used as tumor photosensitizers [16], antibacterial/antimicrobial and anticancer agents [17], radioprotective agents [18], and antidiabetic insulin mimetics [19]. Moreover, the hepato and cardio toxicity induced by some anticancer drugs can be reduced by Zn^{2+} [20].

There is intense interest in the development of molecular systems capable of binding inorganic phosphate anions because of their crucial roles in signal transduction [21,22], energy storage in living organisms, eutrophication of water bodies [23–25], and catalysis [26,27]. Inorganic phosphates exhibit diverse shapes and sizes, hydrophobicity, and high hydration energies, and in some cases, exist only in a limited pH range because of protonation. One phosphate-recognition strategy is the use of metal complexes, mostly involving transition metals, in which the metal ion acts as an anchoring point for the phosphate species. Although different metal ions including transition, lanthanide, and main group metal ions have been used, one of the most commonly used ions for this purpose is Zn^{2+} [28,29].

Phosphate is an indispensable constituent of two important biopolymers—DNA and RNA—and many chemotherapeutic and antiviral drugs [30]. However, the excessive agricultural use of inorganic phosphates causes excessive algal growth, leading to decomposition and decreased dissolved oxygen levels [31]. Dihydrogen phosphate ($H_2PO_4^-$) is the predominant equilibrium species of inorganic phosphates at physiological pH. Therefore, $H_2PO_4^-$ sensing and detection methods have received much attention [32–35]. Phosphate oxoanions such as pyrophosphate play crucial roles in many bioenergetic and metabolic processes such as ATP hydrolysis and DNA or RNA polymerase reactions [36]. The detection of released pyrophosphate has been investigated as a real-time DNA sequencing method [37]. Studies on telomerase activity (a biomarker for cancer) by evaluating the amount of pyrophosphate are also important in cancer research [38]. Furthermore, the pyrophosphate level in synovial fluids has been correlated with the occurrence of calcium pyrophosphate dihydrate disease, a rheumatologic disorder [39]. This species can also be used as a potential biomarker for arthritis [40].

The photophysics of the cation-induced inhibition of excited-state intramolecular proton transfer (ESIPT) has been often used to develop Zn-selective ratiometric emission probes [41–43]. We have previously reported some thiazole-based chemosensors in which the thiazole ring was substituted with a phenol or tosylamide-protected aniline or naphthol at the position 2 and a pyridine, phenyl, or another thiazole

* Corresponding authors.
E-mail addresses: Aasifh@kfupm.edu.sa (A. Helal), kimhs@knu.ac.kr (H.-S. Kim).

http://dx.doi.org/10.1016/j.saa.2016.06.026
1386-1425/

phenol moiety at the position 4 as a ratiometric fluorescence sensor of Zn or dual chemosensor of Zn and Cu [44–50]. We also reported a thiazole-based compound containing a phenol or naphthol at the position 2 and an ester moiety at the position 4 as a very good Al^{3+} sensor [51,52]. Recently, we reported the synthesis of a phenol/naphthol-containing thiazole-based sensor for the sequential detection of Ga and HSO_4^- [53]. In this study, we prepared compound **1** containing a tosylamide-protected aniline at the position 2 of a thiazole ring and an ester moiety at the position 4 (Fig. 1) and investigated its sequential sensing abilities for different cations and anions based on two different mechanisms of fluorescence: ESIPT and chelation-induced enhanced fluorescence (CHEF) [54]. We also synthesized compound **2** to study the effect of the tosyl group in compound **1** on the sensing of cations and anions.

2. Experimental

2.1. General

Melting points were determined using a Thomas-Hoover capillary melting point apparatus and uncorrected. The ^1H and ^{13}C NMR spectra were recorded using a Bruker AM-400 spectrometer and Me_4Si as the internal standard. The FAB mass spectra were obtained at the KBSI Daegu center. The UV–visible absorption spectra were determined using a Shimadzu UV-1650PC spectrophotometer. The fluorescence spectra were measured using a Shimadzu RF-5301 fluorescence spectrometer equipped with a Xe discharge lamp and 1-cm quartz cells with a 5-nm slit width. The IR spectra were recorded using a Shimadzu IR Prestige-21 FTIR spectrometer. All the measurements were carried out at 298 K. Analytical-grade ethanol was purchased from Merck. All other materials for the syntheses were purchased from Aldrich Chemical Co. and used as received without further purification. Compound **3** was obtained following a literature procedure [45], and the quantum yield (Φ) was calculated as reported [53]. The solutions of metal ions were prepared from their analytical-grade perchlorate salts, and those of the anions were prepared from their tetrabutylammonium (TBA) salts. The working solutions were prepared by further dilution of the stock solutions.

2.2. Synthesis

2.2.1. Synthesis of compound *2*

A mixture of compound **3** (200 mg, 0.72 mmol) and 5% Pd/C in ethanol (20 mL) was hydrogenated using H_2 gas for 10 h. After the removal of the solvent, CH_2Cl_2 was added, and the reaction mixture was filtered through a Celite pad to remove the catalyst. The filtrate was concentrated, and the residue was crystalized from a mixture of CH_2Cl_2/hexane, affording amino compound **2** (159 mg, 89% yield). ^1H NMR (DMSO-d_6) δ 1.33 (3H, t, J = 7.1 Hz, CH_3), 4.33 (2H, q, J = 7.1 Hz, CH_2), 6.62 (1H, ddd, J = 7.2, 6.9, 1.0 Hz, H_b), 6.83 (1H, dd, J = 8.3, 1.0 Hz, H_a), 7.11 (1H, s, NH), 7.18 (1H, ddd, J = 7.1, 7.0, 1.4 Hz, H_c), 7.59 (1H, dd, J = 7.9, 1.4 Hz, H_d), 8.47 (1H, s, H_e); 13C NMR (DMSO-d_6) δ 14.2, 60.9, 113.1, 115.7, 116.5, 126.7, 128.9, 131.4, 145.7, 146.7, 160.5, 169.3; HR-FAB MS calcd for $C_{12}H_{13}N_2O_2S$ $(M + H)^+$: 249.0698, found: m/z 249.0699.

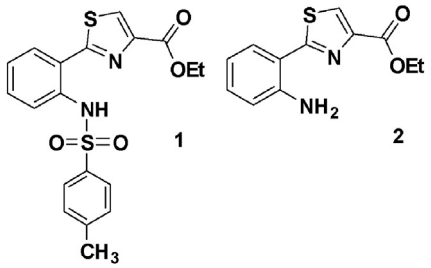

Fig. 1. Structures of chemosensors **1** and **2**.

2.3. Synthesis of compound *1*

Amino compound **2** (100 mg, 0.40 mmol) was added to *p*-toluenesulfonyl chloride (92 mg, 0.48 mol) and triethylamine (0.5 mL) in anhydrous CH_2Cl_2 (20 mL) and stirred at room temperature for 2 h. After the reaction was completed, the mixture was treated with $NaHCO_3$ solution and extracted with CH_2Cl_2. The organic layer was dried and concentrated. The residue was purified by column chromatography (SiO_2, 10% EtOAc in hexane), affording compound **1** (103 mg, 64% yield). Mp. 133 °C (CH_2Cl_2/hexane), TLC R_f 0.35 (10% EtOAc in hexane); ^1H NMR (DMSO-d_6) δ 1.36 (3H, t, J = 7.1 Hz, CH_3), 2.30 (3H, s, CH_3), 4.39 (2H, q, J = 7.1 Hz, CH_2), 7.24 (1H, d, J = 7.6 Hz, H_a), 7.27 (2H, d, J = 8.4 Hz, H_g), 7.42 (2H, t, J = 7.4 Hz, $H_{b,c}$), 7.57 (2H, d, J = 8.4 Hz, H_f), 7.90 (1H, d, J = 7.6 Hz, H_d), 8.64 (1H, s, H_e), 11.45 (1H, s, NH); ^{13}C NMR (DMSO-d_6) δ 14.1, 20.9, 61.1, 121.8, 122.1, 125.3, 126.7, 129.2, 129.3, 129.7, 131.4, 134.9, 135.9, 143.7, 145.3, 160.2, 166.6; HR-FAB MS calcd for $C_{19}H_{19}N_2O_4S_2$ $(M + H)^+$: 403.0786, found: m/z 403.0788.

2.3.1. Synthesis of *1*-*Zn* complex

A mixture of compound **1** (40 mg, 0.10 mmol) and $Zn(NO_3)_2 \cdot 6H_2O$ (30 mg, 0.10 mmol) in ethanol/CH_2Cl_2 (5:5 v/v, 5 mL) was stirred for 1 h. The mixture was stand at room temperature, and the precipitated complex was filtered off. The filtered cake was washed thoroughly with ethanol and dried under vacuum, providing the complex (43 mg, 91% yield). HR-FAB mass: calcd for $[C_{19}H_{17}N_2O_4S_2Zn]^+$ 464.9921. Found: 464.9920.

2.4. UV–visible and fluorescence studies

A solution of host (30 μM) in EtOH was prepared, and the guest (300 μM) solution was added to the host solution for the UV–visible study. For fluorescence titration, a solution of host (3 μM) in EtOH was prepared, and the guest (30 μM) solution was added to the host solution. In a typical titration experiment, 2 mL of the host solution was transferred to a fluorescence cell, and the emission spectrum was recorded at a fixed wavelength. The guest solution (20 μL) was added through a microsyringe, and the amount was increased until 10 equiv of guest. The fluorescence spectrum of each solution was recorded after each addition. The association constants were determined by gnuplot using the following equation.

plot “gadata.dat” u 1:2 w lp.
f(x) = (a + b * c * x * * 1.00) / (1 + c * x * * 1.00).
fit f(x) “gadata.dat” u 1:2 via a, b, and c.

2.5. Theoretical calculations

The geometry of sensor **1** was optimized using gradient-correlated density functional theory (DFT) according to literature [55–59].

3. Results and discussion

3.1. Synthesis of sensor *1*

The required compound **2** was prepared by the reduction of ethyl 2-(2′-nitrophenyl)thiazoly-4-carboxylate, which was obtained by the reaction of 2-nitrothiobenzamide with ethyl bromopyruvate in ethanol [45]. Compound **1** was prepared by the reaction of compound **2** with *p*-toluenesulfonyl chloride in the presence of triethylamine in a good yield (Scheme 1). The ^1H NMR spectrum of sensor **1** in DMSO-d_6 showed CH_3CH_2 signals corresponding to the ethyl ester—a triplet at δ 1.36 and a quartet at δ 4.49—as well as one singlet corresponding to the tosyl CH_3 at δ 2.30 and one N–H singlet at δ 11.45. In the ^{13}C NMR

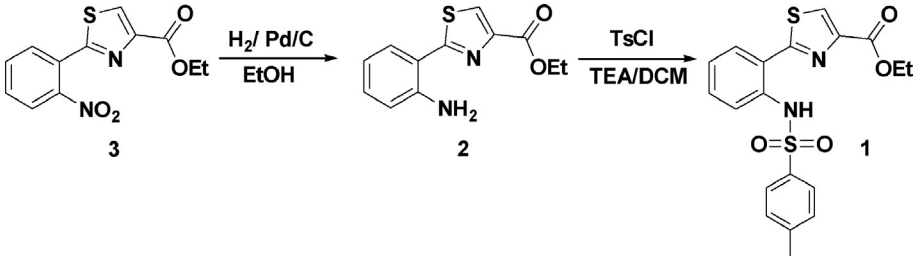

Scheme 1. Synthesis of sensor **1**.

spectrum of sensor **1**, the signal of ethyl ester appeared at δ 14.1 and 61.1, and the tosyl CH_3 signal was observed at δ 20.9. The high-resolution mass spectrum (HRMS) of sensor **1** showed a molecular ion peak of $(M + H)^+$ at $m/z = 403.0788$ (see ESI).

*3.2. UV–visible and fluorescence studies of sensor **1** in the presence of metal ions*

The initial studies on the UV–visible absorption and fluorescence emission of ethyl 2-(2′-tosylamidophenyl)-4-thiazole carboxylate, sensor **1**, were carried out in EtOH. Among the tested solvents, ethanol showed the best response for sensor **1** in the UV–vis spectrum (Fig S4). The binding of sensor **1** to Zn^{2+} in the form of perchlorate salt was investigated by UV–visible spectroscopy. In the absence of Zn, sensor **1** showed absorption bands with maxima at 286 nm (log ε = 3.98) and 318 nm (log ε = 3.76), whereas the addition of Zn^{2+} to compound **1** resulted in a red shift of the absorption band maxima to 296 nm (log ε = 3.96) and 369 nm (log ε = 3.53) (Fig. 2a). The absorption band at 318 can be attributed to the *n*–π* transition resulting from the intramolecular hydrogen bonding involving the lone pair electrons on the nitrogen of the thiazole ring, whereas the red shift to 369 nm can be attributed to the favored planar orientation of the complex caused by metal binding and inhibition of ESIPT [60]. The peak at 288 nm originates from the π–π* transition of the aromatic rings.

Sensor **1** showed weak fluorescence with a low quantum yield (Φ = 0.0059) at 382 nm and 535 nm, corresponding to the enamine and ketamine peaks, respectively, resulting from ESIPT. The introduction of Zn^{2+} leads to the formation of a stable complex with sensor **1** that inhibits the ESIPT, and consequently the chelated system produce an emission band at 460 nm with a larger quantum yield (Φ = 0.0653) due to CHEF (Fig. 2b) [54]. Similar UV–visible and fluorescence studies of sensor **2** towards various metal ions did not show any significant selectivity and sensitivity because ESIPT is not possible in compound **2** because of the low acidity of the free amine compared to that of the tosylamide-protected compound **1** (Fig. S5).

The UV–visible titration of sensor **1** was performed in EtOH. The absorption bands of compound **1** linearly increased and decreased up to 1 equiv of Zn^{2+} (Fig. 3a), indicating the formation of a 1:1 complex with a high binding affinity. This finding is characteristic for the 2-(2′-tosylaminophenyl)thiazole derivatives when the complexation is accompanied by the deprotonation of the N–H proton [45]. Moreover, three clearly defined isosbestic points (294 nm, 313 nm, and 337 nm) were observed in the titration spectra of compound **1**, indicating the conversion of free sensor **1** to the corresponding Zn^{2+} complex [61, 62]. The binding constant of the complex between sensor **1** and Zn^{2+} was determined by the nonlinear fitting of the corresponding UV–visible titration data and yielded a value of $1.06 \times 10^4\ M^{-1}$ with a satisfactory correlation coefficient (R = 0.9983) [63]. The error was estimated to be ≤7%. The fluorescence titration of compound **1** with Zn^{2+} was also performed. The emission band of compound **1** linearly increased up to 1 equiv of Zn^{2+} (Fig. 3b). To further quantify the complexation ratio of sensor **1** with Zn^{2+} in the complex, Job's method was used, considering the emission changes at 460 nm as a function of the molar fraction of Zn^{2+}. The maximum emission was observed when the molar fraction of Zn^{2+} reached 0.5, indicating a 1:1 stoichiometry in the sensor **1**-Zn^{2+} complex (Fig. S6). The change in the color of the fluorescence after the introduction of Zn^{2+} was observed mainly because of the inhibition of ESIPT. Then, Zn^{2+}, which is prone to bind to the sulfonyl oxygen of the tosyl group, oxygen of the ester group, nitrogen of the thiazole ring, and deprotonated nitrogen of the amide, preferentially forms a stable chelated complex. Thus, the ESIPT ceases, and CHEF plays the key role, resulting in an emission at 460 nm. The preferential binding of Zn^{2+} with the oxygen of the tosyl and ester group, nitrogen of the thiazole ring, and amide group was also established by the energy-minimized structure of sensor **1**-Zn^{2+} complex using B3LYP/6-31G* set in Fig. 9.

The selectivity is one of the important criteria for the potential application of a cation sensor. To determine the selectivity of sensor **1**, 10 equiv of various biologically and non-biologically relevant metal cations were added to a solution of compound **1** (10 μM), and their binding was investigated by fluorescence spectroscopy. No cations other than

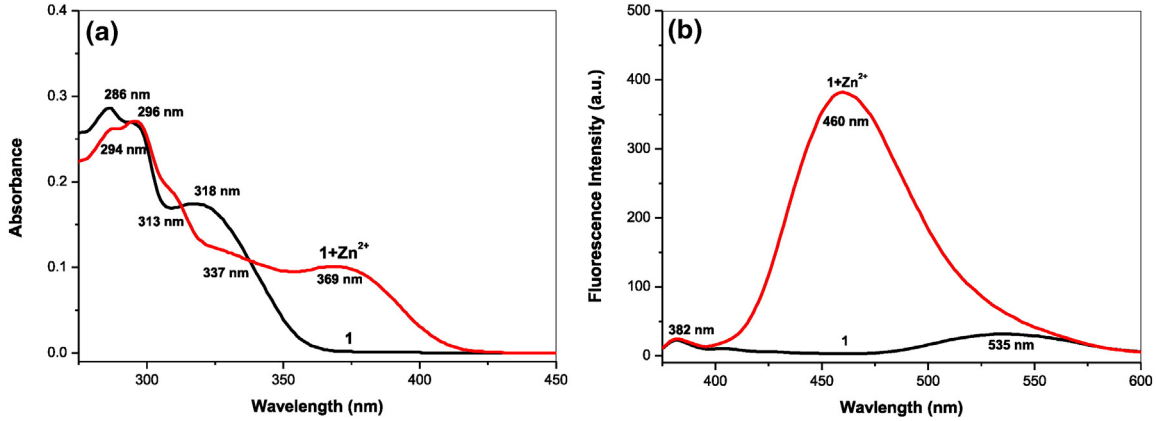

Fig. 2. (a) UV–visible spectra of compound **1** (30 μM) with 10 equiv of $Zn(ClO_4)_3$ and (b) fluorescence spectra of compound **1** (10 μM) with 10 equiv of $Zn(ClO_4)_2$ in EtOH. $\lambda_{ex} = 337$ nm.

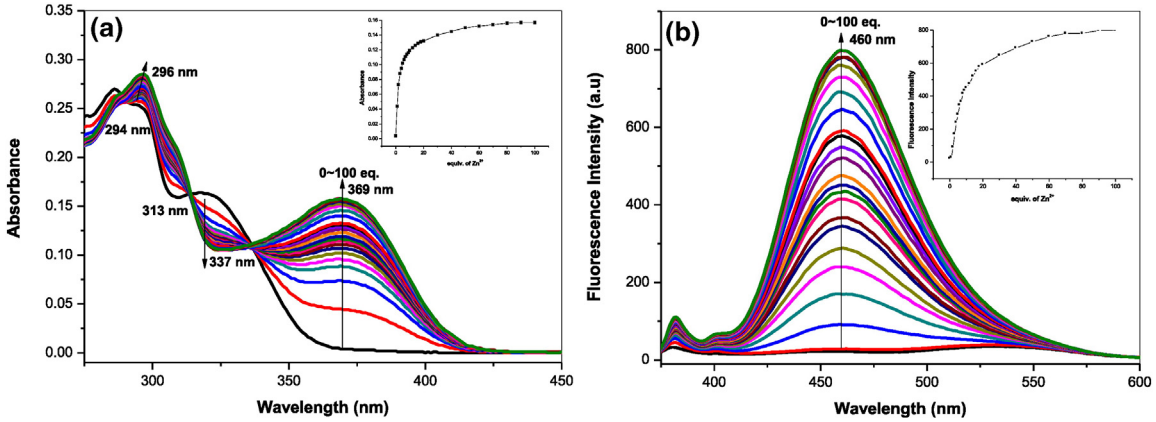

Fig. 3. (a) UV–visible spectra of compound **1** (30 μM) titrated with $Zn(ClO_4)_2$ from 0 to 100 equiv in EtOH. Inset plots represent the dependence of the absorbance intensity at 369 nm upon the addition of $Zn(ClO_4)_2$. (b) Fluorescence titration of compound **1** (10 μM) with $Zn(ClO_4)_2$ in EtOH, $\lambda_{ex} = 337$ nm. Inset plots represent the dependence of the fluorescence intensity at 460 nm upon the addition of $Zn(ClO_4)_2$.

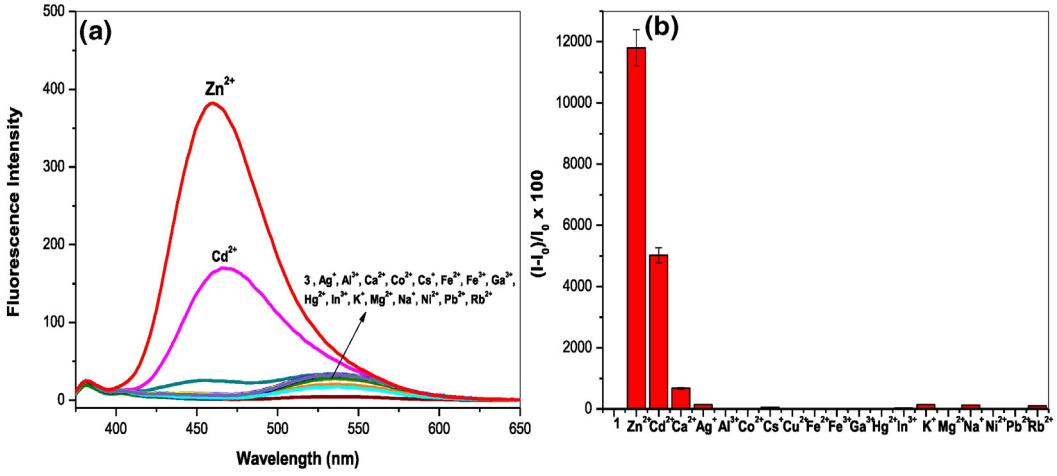

Fig. 4. (a) Fluorescence spectra of compound **1** (10 μM) with 10 equiv of various cations in EtOH. ($\lambda_{ex} = 337$ nm, $\lambda_{em} = 460$ nm). (b) Fluorescence intensity of compound **1** with various cations in EtOH at $\lambda_{em} = 460$ nm.

Zn^{2+}, which produced a prominent fluorescence signal, induced any distinct emission shift in the spectra of compound **1**, except Cd^{2+} (Fig. 4). The addition of Cd^{2+}, which has coordination properties similar to those of Zn^{2+}, produced a slight change in the emission spectra. Competition experiments were performed to explore the possibility of using compound **1** as a practical ion-selective fluorescent chemosensor for Zn^{2+}. In these experiments, compound **1** (10 μM) was first mixed with 10 equiv of Zn^{2+}, followed by the addition of 10 equiv of various competing metal ions. The fluorescence emission spectra showed that most of the common metal ions exhibited no clear interference with the detection of Zn^{2+} (Fig. S7). The plot of the linear relationship between fluorescence intensity at 460 nm vs. $[Zn^{2+}]$ during the

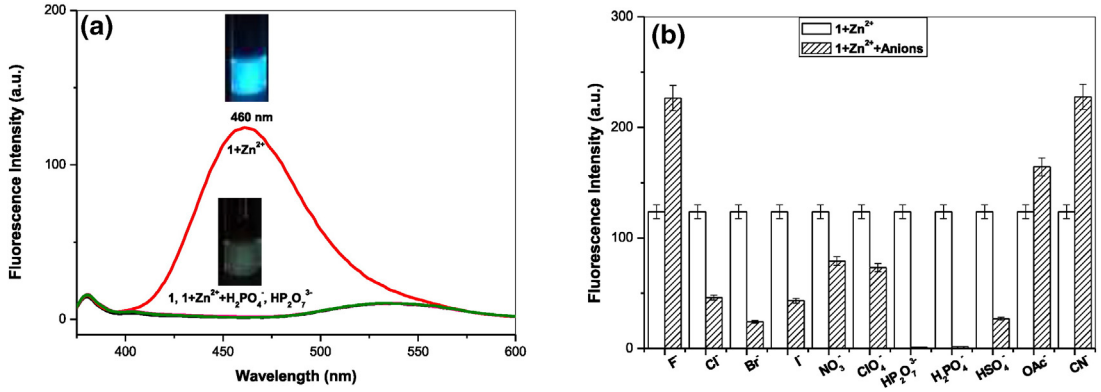

Fig. 5. (a) Fluorescence spectra of compound **1** (3 μM) upon the addition of Zn^{2+} (10 equiv) and subsequent addition of anions (10 equiv). (b) Fluorescence responses of **1**-Zn^{2+} in the presence of various anions (10 equiv) in EtOH. The white bars represent emission upon the addition of 10 equiv of Zn^{2+} to compound **1** (3 μM). The shaded bars represent the change in emission that occurs upon the subsequent addition of 10 equiv of various anions to a 3 μM solution of **1**-Zn^{2+}. $\lambda_{ex} = 337$ nm. $\lambda_{em} = 460$ nm.

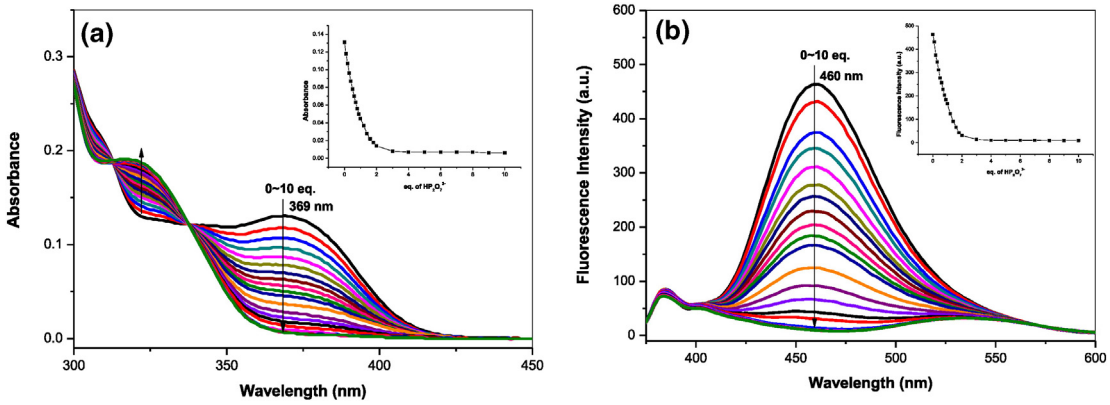

Fig. 6. (a) UV–visible titrations of **1**-$\mathbf{Zn^{2+}}$ complex (30 μM) with $HP_2O_7^{3-}$ (10 equiv) in EtOH. Inset plots represent the relationship between the absorbance intensity at 369 nm and the $HP_2O_7^{3-}$ concentration. (b) Fluorescence titrations of **1**-$\mathbf{Zn^{2+}}$ complex (10 μM) with $HP_2O_7^{3-}$ (10 equiv) in EtOH. Inset plots represent the relationship between the fluorescence intensity at 460 nm and the $HP_2O_7^{3-}$ concentration.

Table 1
Binding constants *Ka* (M^{-1}) of **1**-$\mathbf{Zn^{2+}}$ and with anions[a].

	UV	Fluorescence
1-$\mathbf{Zn^{2+}}$	1.06×10^4	0.98×10^4
1-$\mathbf{Zn^{2+}}$-$HP_2O_7^{3-}$	1.46×10^5	1.40×10^5
1-$\mathbf{Zn^{2+}}$-$H_2PO_4^-$	5.20×10^5	5.66×10^5

[a] Estimated errors are 7–16%.

fluorescence titrations of sensor **1** (10 μM) with $Zn(ClO_4)_2$ (100 equiv) showed that the limit of detection of Zn^{2+} by sensor **1** was 20 μM in EtOH (R = 0.981) (Fig. S8) [63].

3.3. Fluorescence based selectivity of **1**-$\mathbf{Zn^{2+}}$ ensemble towards anions

The binding of sensor **1** with Zn^{2+} was weak compared to the other thiazole-based sensors reported previously (Table S1) [44,45,48]. Therefore, the anion selectivity of **1**-$\mathbf{Zn^{2+}}$ ensemble was investigated. Because $H_2PO_4^-$ and $HP_2O_7^{3-}$ can form strong complexes with Zn^{2+}, the use of **1**-$\mathbf{Zn^{2+}}$ complex as a chemosensor for the detection of $HP_2O_7^{3-}$ and $H_2PO_4^-$ was investigated. Complex **1**-$\mathbf{Zn^{2+}}$ (3 μM) was treated with 10 equiv of various anions including F^-, Cl^-, Br^-, I^-, NO_3^-, ClO_4^-, $H_2PO_4^-$, $HP_2O_7^{3-}$, OAc^-, and CN^-. As shown in Fig. 5, the addition of $HP_2O_7^{3-}$ and $H_2PO_4^-$ caused remarkable complete fluorescence quenching, whereas the addition of F^-, OAc^-, and CN^- enhanced the fluorescence. Because of the high Zn-phosphate affinity, the addition of $HP_2O_7^{3-}$ and $H_2PO_4^-$ caused the disappearance of the peak at 460 nm, and the enamine and ketamine peaks appeared at 382 nm and 535 nm by displacing Zn^{2+} from sensor **1** and restoring ESIPT, which had been inhibited by Zn^{2+}. In contrast, the addition of F^-, OAc^-, and CN^- enhanced the fluorescence by displacing the ligand and removing the acidic N–H proton, thereby inhibiting ESIPT. Competition experiments were performed to investigate whether this property of **1**-$\mathbf{Zn^{2+}}$ was influenced by CN^- or any other anions at concentrations exceeding the concentrations of $HP_2O_7^{3-}$ and $H_2PO_4^-$ by as much as 10 times. These experiments showed that **1**-$\mathbf{Zn^{2+}}$ complex had a high selectivity and sensitivity for $HP_2O_7^{3-}$ and $H_2PO_4^-$ ions.

Upon the slow addition of $HP_2O_7^{3-}$, the peak at 460 nm, resulting from the addition of Zn^{2+} to compound **1**, was gradually quenched because of the disappearance of CHEF and restoration of ESIPT until a total of 1 equiv of $HP_2O_7^{3-}$ was added. A further increase in the $HP_2O_7^{3-}$-concentration did not lead to any additional quenching. The binding constants of **1**-$\mathbf{Zn^{2+}}$ to $HP_2O_7^{3-}$ as determined by UV–visible and fluorescence titrations were 1.46×10^5 M^{-1} and 1.40×10^5 M^{-1}, respectively. (Fig. 6 and Table 1). The emission intensity of **1**-$\mathbf{Zn^{2+}}$ at 460 nm steadily decreased until a total of 1 equiv of $HP_2O_7^{3-}$ was added (inset plot in Fig. 6b). The Job's plot showed a 1:1 stoichiometry between **1**-$\mathbf{Zn^{2+}}$ and $HP_2O_7^{3-}$ (Fig. S9). The same results were obtained from the UV–visible and fluorescence titrations of **1**-$\mathbf{Zn^{2+}}$ with $H_2PO_4^-$ (Fig. S10). However, the fluorescence titration of **2**-$\mathbf{Zn^{2+}}$ (10 μM) with 10 equiv of anions did not show any significant activity (Fig. S11).

A linear decrease in the fluorescence intensity of sensor **1**-$\mathbf{Zn^{2+}}$ at 460 nm upon the gradual addition of a solution of $HP_2O_7^{3-}$ and $H_2PO_4^-$ indicated the limits of detection of $HP_2O_7^{3-}$ and $H_2PO_4^-$ as 1 μM and 1 μM, respectively for **1**-$\mathbf{Zn^{2+}}$ (R^1 = 0.986 for $HP_2O_7^{3-}$, and R^2 = 0.971 for $H_2PO_4^-$) in EtOH (Fig. S12). [63].

The complexation properties of **1**-$\mathbf{Zn^{2+}}$ complex were further studied by fluorescence. The addition of up to 10 equiv of CN^- to **1**-$\mathbf{Zn^{2+}}$

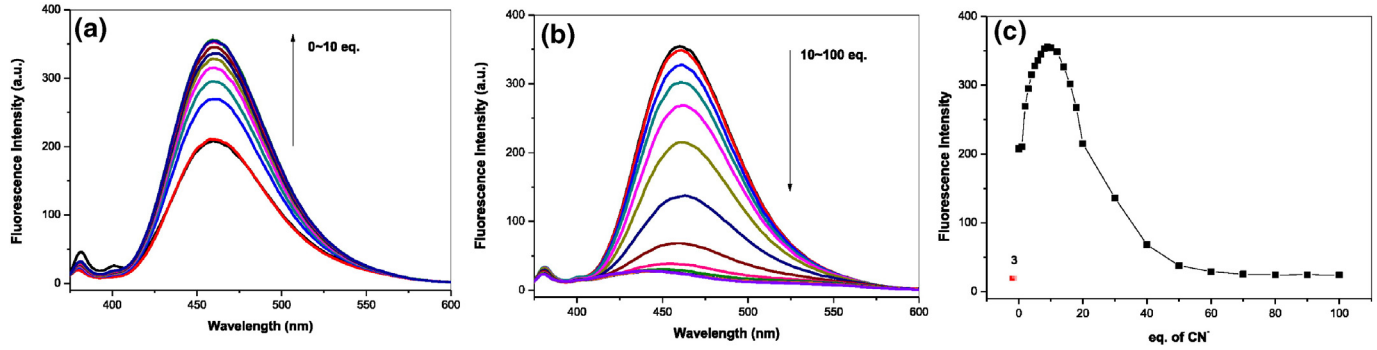

Fig. 7. Fluorescence changes in **1**-$\mathbf{Zn^{2+}}$ (1:10, 3 μM) upon the addition of (a) 0–10 equiv and (b) 10–100 equiv of CN^- in EtOH. (c) Plots represent the relationship between the emission intensity at 460 nm and the concentration of CN^-.

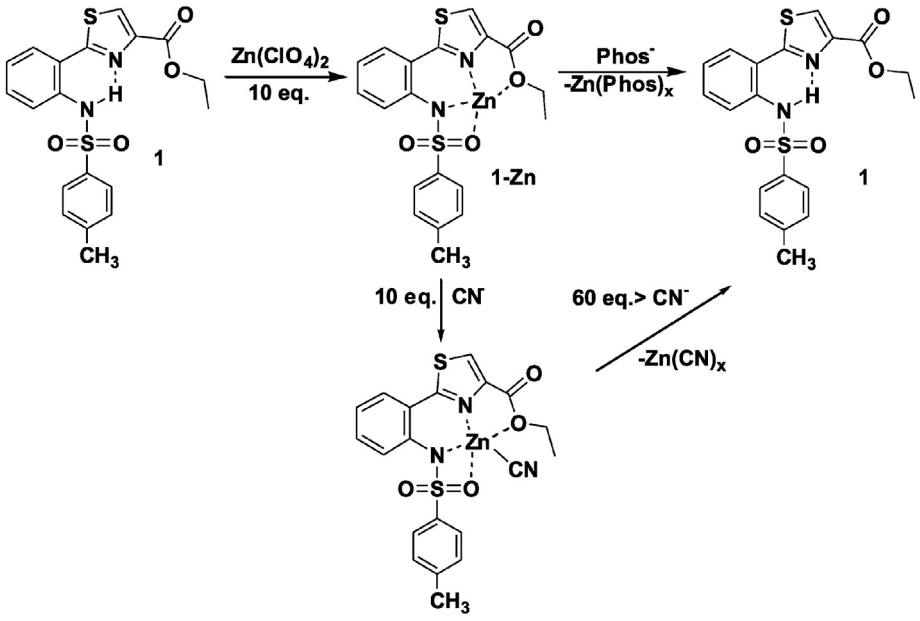

Scheme 2. Plausible complexation mechanism between sensor **1**, Zn^{2+}, and anions.

complex in solution (3 μM) enhanced the fluorescence, due to the enhancement of the CHEF on anion binding with the metal of the **1**-$\mathbf{Zn^{2+}}$ *complex*, and with further addition of up to 60 equiv of CN^-, the emission intensity gradually decreased, the fluorescence was quenched, and peaks appeared at 382 nm and 535 nm, resulting from the displacement of Zn^{2+} from **1**-$\mathbf{Zn^{2+}}$ complex that inhibits the CHEF mechanism and restores the ESIPT (Fig. 7, Scheme 2). Similar trends were observed in the fluorescence spectra of **1**-$\mathbf{Zn^{2+}}$ upon the addition of 10–100 equiv of F^- (Fig. S13).

3.4. NMR binding study

To further investigate the nature of Zn binding to sensor **1**, a ^{1}H NMR study of sensor **1** in the presence of Zn^{2+} was performed in CD_3CN. The addition of 1–2 equiv of $Zn(ClO_4)_2$ to a solution of sensor **1** in CD_3CN did not produce any significant shifts in any of the proton signals.

The ^{1}H NMR study of sensor **1** was performed in the presence of Zn^{2+} in CD_3CD_2OD. The ^{1}H NMR spectra of compound **1** showed no sulfonamide NH proton, which was exchanged with deuterio-ethanol, whereas all other protons, i.e., the signals of aminophenyl protons H_a, H_b, H_c, and H_d, and *p*-tosylamide protons H_f, H_g, and H_h shifted downfield except the proton of thiazole H_e that shifted upfield compared to its ^{1}H NMR spectra in DMSO-d_6 (Fig S1). The addition of 2 equiv of $Zn(ClO_4)_2$ to a solution of compound **1** showed 7% complex formation, as obtained from the integration of the complexed and free proton H_e. The addition of 5 equiv of $Zn(ClO_4)_2$ to a solution of compound **1** triggered ~11% of complex formation and showed significant upfield shifts of the aminophenyl protons H_a, H_b, and H_c from δ 7.199 to 6.930 ppm (H_a), δ 7.735 to 7.533 ppm (H_b), and δ 7.433 to 7.257 ppm (H_c), respectively, and the other proton H_d shifted downfield from δ 7.790 to 7.911 ppm. Thiazole proton H_e, and *p*-tosyl protons H_f, H_g, and H_h shifted downfield from δ 8.396, 7.571, 7.131, and 2.285 ppm to 8.726, 7.742, 7.324, and 2.381 ppm, respectively (Fig. 8). Moreover, the ethoxy methylene proton also shifted from δ 4.464 ppm to δ 4.566 ppm (Fig. S14). These NMR chemical shifts explain the chelation effect of Zn^{2+} with sensor **1**. Further addition of 100 equiv of Zn^{2+} to a solution of

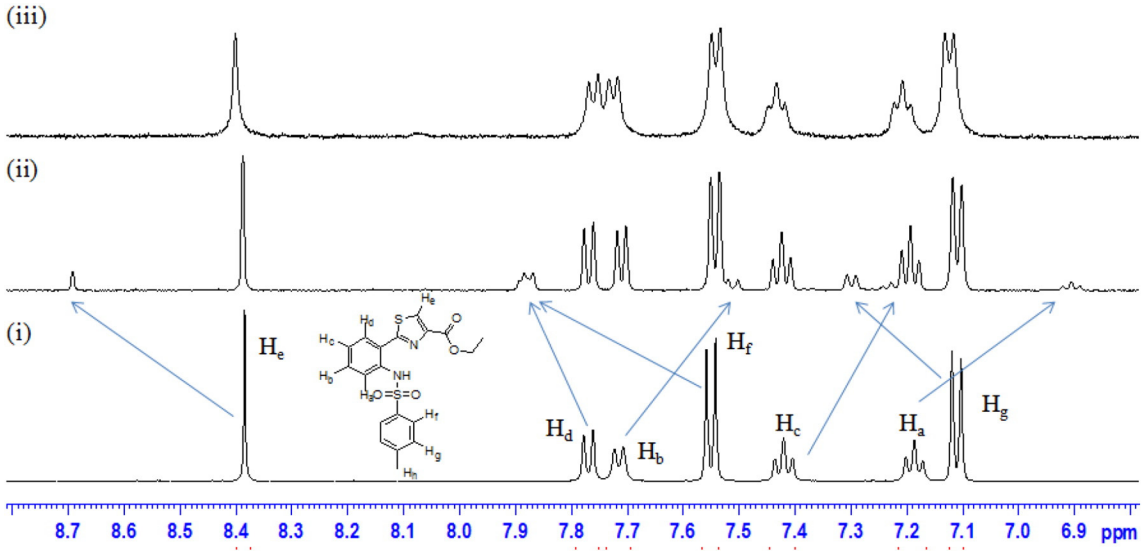

Fig. 8. A partial ^{1}H NMR spectra of compound **1** (4.5 μM) in CD_3CD_2OD at 25 °C: (i) Free **1**, (ii) **1** + Zn^{2+} (5 equiv), and (iii) **1** + Zn^{2+} (5 equiv) + $H_2PO_4^-$ (10 equiv).

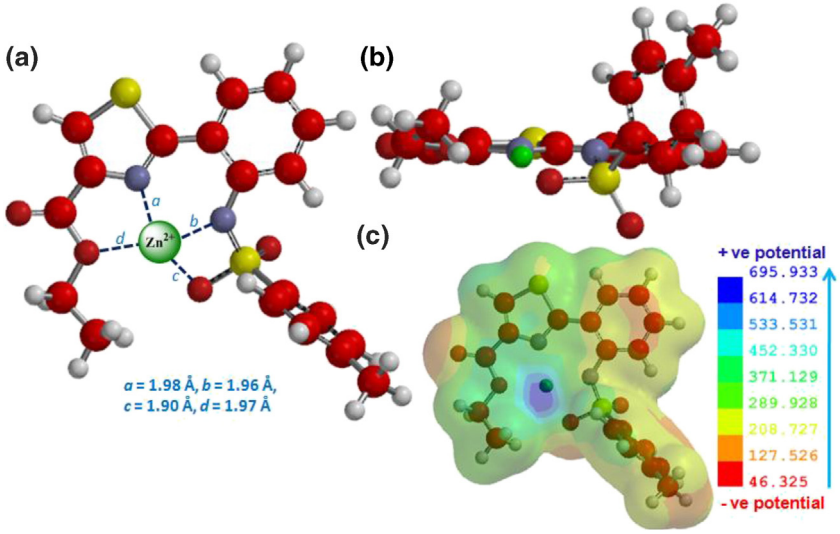

Fig. 9. DFT based energy-minimized structure of **1**-$\mathbf{Zn}^{2+}$ complex using B3LYP/6-31 G* as the basis set in EtOH as an implicit medium; a) vertical view, b) horizontal view, and c) complex electrostatic potential map (the blue to red trend shows the positive to negative potential property range in kJ/mol). (For interpretation of the references to color in this figure legend, the reader is referred to the web version of this article.)

compound **1** formed 21% of complex with band broadening. These results clearly indicate that the formation of a complex between compound **1** and Zn^{2+} was very weak in CD_3CD_2OD. The addition of $H_2PO_4^-$ (10 equiv) to the resulting mixture of sensor **1** and Zn^{2+} (5 equiv) regenerated sensor **1** by removing Zn^{2+} from **1**-$\mathbf{Zn}^{2+}$ complex as $Zn(H_2PO_4)$ is shown in Fig. 8.

3.5. IR and HRMS study

A complex of sensor **1** with $Zn(NO_3)_2$ in a mixture of ethanol/CH_2Cl_2 (5:5 v/v) was prepared and characterized by IR (KBr) and HR-FAB mass. The IR spectrum of compound **1** showed a characteristic N–H stretching at 3142 cm^{-1}, ester C═O stretching at 1732 cm^{-1}, and thiazole C═N stretching at 1602 cm^{-1}. Complex **1**-**Zn** showed the disappearance of N–H stretching at 3142 cm^{-1} due to N–Zn formation (Figs. S15–S16). The HRMS spectra of complex **1**-**Zn** showed a 1:1 stoichiometry with the molecular ion peak at m/z 464.9920, corresponding to [**1** + **Zn**-**1**]$^+$ (Fig. S17). These data confirmed the 1:1 formation of **1**-**Zn** complex.

3.6. DFT study

To understand the complexation of Zn^{2+} with sensor **1**, B3LYP/6-31G* level energy minimization calculation was performed using SPARTAN 10 software in ethanol (SM8 solvent model) as the implicit medium [55–59]. The calculated energy-minimized structure of **1**-$\mathbf{Zn}^{2+}$ complex indicated the interaction distances between Zn^{2+} and the deprotonated nitrogen of the sulfonamide (because of a higher resonance stabilization through complexation) (b), nitrogen of the thiazole ring (a), sulfonyl oxygen of the tosyl group (c), and oxygen of the ester ethoxy group (d) in Fig. 9. A distance of 1.90 Å and 1.96 Å were calculated for the Zn—O bond (c) between the tosyl S–O and Zn–N bonds (b) between the deprotonated N and Zn^{2+}. Other two interactions between Zn^{2+} and thiazole C═N and the oxygen of ethoxy ester group were calculated to be 1.97 Å and 1.98 Å, respectively. The band-gap energies ($-\Delta E_{HOMO-LUMO}$) of sensor **1** ($-\Delta E_1$ = 4.01 eV) was higher than that of Zn^{2+} complex ($-\Delta E^{2+}_{\mathbf{1\text{-}Zn}}$ = 3.80 eV), indicating that the complexation is thermodynamically stable (Fig. S18). The higher electron polarization of the N–S–O bond towards the oxygen atom in tosyl amide makes stronger donating capacity than the nitrogen atom, as visualized through the decreased bond distance between the latter to former as well as in the electrostatic potential map (Fig. 9c). Moreover, a spatial orientation of the donor atoms of sensor **1**, specifically N, O (sulfonyl group), N (thiazole), and O (ester) as well as Zn^{2+} ions were located on the same plane (Fig. 9b), indicating that sensor **1** formed a stable chelated complex. Thus, CHEF plays the key role in the emission at 460 nm.

The applications of sensor **1** to detect metal ions including Zn^{2+} and anions in real analytes will be carried out in due course.

4. Conclusions

In conclusion, a highly Zn-selective 2-(2′-tosylamidophenyl)thiazole-based fluorescent chemosensor **1** was synthesized. Sensor **1** showed a highly selective "on–off"-type fluoroionophoric switching behavior towards Zn^{2+}, and partial enhancement with Cd^{+2} even in the presence of diverse common interfering metals ions such as Co^{+2}, Ni^{2+}, and Cu^{+2}. The fluorescence was based on ESIPT followed by CHEF mechanism. Moreover, **1**-$\mathbf{Zn}^{2+}$ complex showed a high selectivity and sensitivity towards $HP_2O_7^{3-}$ and $H_2PO_4^-$ that completely quenched the fluorescence of the complex by displacing the Zn^{2+}.

Acknowledgment

This research was supported by the Basic Science Research Program through the National Research Foundation of Korea (NRF) funded by the Ministry of Science, ICT, and Future Planning (2013R1A1A2006777).

Appendix A. Supplementary data

Supplementary data to this article can be found online at http://dx.doi.org/10.1016/j.saa.2016.06.026.

References

[1] A.D. Cort, G. Forte, L. Schiaffino, J. Organomet. Chem. 76 (2011) 7569–7572.
[2] Y.P. Li, H.R. Yang, Q. Zhao, W.C. Song, J. Han, X.H. Bu, Inorg. Chem. 51 (2012) 9642–9648.
[3] Y.L. Yang, Y.W. Wang, Y. Peng, Sci. China Chem. 57 (2014) 289–295.
[4] E.L. Que, D.W. Domailli, C.J. Chang, Chem. Rev. 108 (2008) 1517–1549.
[5] R.M. Manez, F. Sancenon, Chem. Rev. 103 (2003) 4419–4476.
[6] J.S. Kim, D.T. Quang, Chem. Rev. 107 (2007) 3780–3799.
[7] P. Jiang, Z. Guo, Coord. Chem. Rev. 248 (2004) 205–229.
[8] P.D. Zalewski, I.J. Forbes, G. Mazdai, C. Giannakis, Biochem. Int. 24 (1991) 1093–1101.
[9] J.J. Frausto da Silva, R.J.P. Williams, The Biological Chemistry of the Elements, Clarendon Press, Oxford, 1991 302.

[10] X.M. Xie, T.G. Smart, Nature 349 (1991) 521–524.
[11] D.W. Choi, J.Y. Koh, Annu. Rev. Neurosci. 21 (1998) 347–375.
[12] R.J. Cousins, L.M. Lee-Ambrose, J. Nutr. 122 (1992) 56–64.
[13] L. Harrison, S.J. Gibbons, Neuropharmacology 33 (1994) 935–1038.
[14] F. Grummt, C. Wienmann-Dorsch, J. Schneider-Schaulies, A. Lux, Exp. Cell Res. 163 (1986) 191–200.
[15] B.L. Vallee, K.H. Falchuk, Physiol. Rev. 73 (1993) 79–118.
[16] Q. Huang, Z. Pan, P. Wang, Z. Chen, X. Zhang, H. Xu, Bioorg. Med. Chem. Lett. 16 (2006) 3030–3033.
[17] S. Anbu, S. Kamalraj, B. Varghese, J. Muthumary, M. Kandaswamy, Inorg. Chem. 51 (2012) 5580–5592.
[18] S. Emami, S.J. Hosseinimehr, S.M. Taghdisi, S. Akhlaghpoor, Bioorg. Med. Chem. Lett. 17 (2007) 45–48.
[19] H. Sakurai, Y. Yoshikawa, H. Yasui, Chem. Soc. Rev. 37 (2008) 2383–2392.
[20] M.M. Ali, E. Frei, J. Straubb, A. Breuerb, M. Wiesslerb, Toxicology 179 (2002) 85–93.
[21] M.W. Bowler, M.J. Cliff, J.P. Waltho, G.M. Blackburn, New J. Chem. 34 (2010) 784–794.
[22] E.A. Katayev, Y.A. Ustynyuk, J.L. Sessler, Coord. Chem. Rev. 250 (2006) 3004–3037.
[23] J. Yoon, S.K. Kim, N.J. Singh, K.S. Kim, Chem. Soc. Rev. 35 (2006) 355–360.
[24] J.W. Steed, Chem. Commun. (2006) 2637–2649.
[25] P.A. Gale, Chem. Commun. 47 (2011) 82–86.
[26] B.E. Turk, Curr. Opin. Chem. Biol. 12 (2008) 4–10.
[27] J.P. Morrow, T.L. Amyes, J.P. Richard, Acc. Chem. Res. 41 (2008) 539–548.
[28] A.E. Hargrove, S. Nieto, T. Zhang, J.L. Sessler, E.V. Anslyn, Chem. Rev. 111 (2011) 6603–6782.
[29] A. Gogoi, S. Mukherjee, A. Ramesh, G. Das, RSC Adv. 5 (2015) 63634–63640.
[30] A. Ojida, Y. Mito-oka, K. Sada, I. Hamachi, J. Am. Chem. Soc. 126 (2004) 2454–2463.
[31] P.A. Gale, Chem. Commun. 30 (2005) 3761–3772.
[32] A. Gogoi, S. Samanta, G. Das, Sensors Actuators B 202 (2014) 788–794.
[33] C. Bazzicalupi, A. Bencini, V. Lippolis, Chem. Soc. Rev. 39 (2010) 3709–3728.
[34] C. Warwick, A. Guerreiro, A. Soares, Biosens. Bioelectron. 41 (2013) 1–11.
[35] T. Lawal, S.B. Adeloju, Talanta 114 (2013) 191–203.
[36] C.P. Mathews, K.E. van Hold, Biochemistry, The Benjamin/Cummings Publishing Company, Inc., Redwood City, CA, 1990.
[37] M. Ronaghi, S. Karamohamed, B. Pettersson, M. Uhle´n, P. Nyre´n, Anal. Biochem. 242 (1996) 84–89.
[38] S. Xu, M. He, H. Yu, X. Cai, X. Tan, B. Lu, B. Shu, Anal. Biochem. 299 (2001) 188–193.
[39] A.E. Timms, Y. Zhang, R.G. Russell, M.A. Brown, Rheumatology 41 (2002) 725–729.
[40] R.A. Terkeltaub, Am. J. Phys. Cell Physiol. 281 (2001) C1–C11.
[41] M.M. Henary, C.J. Fahrni, J. Phys. Chem. A. 106 (2002) 5210–5220.
[42] M.M. Henary, Y.G. Wu, C.J. Fahrni, Chem. Eur. J. 10 (2004) 3015–3025.
[43] M.M. Henary, Y. Wu, J. Cody, S. Sumalekshmy, J. Li, S. Mandal, C.J. Fahrni, J. Organomet. Chem. 72 (2007) 4784–4797.
[44] A. Helal, H.-S. Kim, Tetrahedron Lett. 50 (2009) 5510–5515.
[45] A. Helal, S.H. Kim, H.-S. Kim, Tetrahedron 66 (2010) 9925–9932.
[46] A. Helal, S.H. Lee, S.H. Kim, H.-S. Kim, Tetrahedron 66 (2010) 7097–7103.
[47] A. Helal, S.H. Lee, S.H. Kim, H.-S. Kim, Tetrahedron Lett. 51 (2010) 3531–3688.
[48] A. Helal, M.H.O. Rashid, C.H. Choi, H.-S. Kim, Tetrahedron 68 (2012) 647–653.
[49] A. Helal, H.-S. Kim, Spectrochim. Acta Part A 105 (2013) 273–279.
[50] A. Helal, M.H.O. Rashid, C.H. Choi, H.-S. Kim, Tetrahedron 67 (2011) 2794–2802.
[51] A. Helal, S.H. Kim, H.-S. Kim, Tetrahedron 69 (2013) 6069–6095.
[52] A. Helal, H.G. Kim, M.K. Ghosh, C.-H. Choi, H.-S. Kim, Tetrahedron 69 (2013) 9600–9608.
[53] B.-Y. Kim, H.-S. Kim, A. Helal, Sensors Actuators B 206 (2015) 430–434.
[54] S. Das, S. Goswami, K. Aich, K. Ghoshal, C.K. Quah, M. Bhattacharyya, H.-K. Fun, New J. Chem. 39 (2015) 8582–8587.
[55] Spartan. Wavefunction, Inc., http://www.wavefun.com/index.html;2008.
[56] A. Pandith, A. Kumar, H.-S. Kim, RSC Adv. 5 (2015) 81808–81816.
[57] G.P. Shusterman, A.J. Shusterman, Teaching chemistry with electron density models, J. Chem. Educ. 74 (1997) 771–776.
[58] D.G. Truhlar, in: P. Politzer (Ed.), Chemical Applications of Atomic and Molecular Electrostatic Potentials, Plenum, New York, 1981.
[59] C. Lee, W. Yang, R.G. Parr, Development of the Colle-Salvetti correlation-energy formula into a functional of the electron density, Phys. Rev. B Condens. Matter 37 (1988) 85–89.
[60] J. Keck, H.E.A. Kramer, H. Port, T. Hirsch, P. Fischer, G. Rytz, J. Phys. Chem. 100 (1996) 14468–14475.
[61] G. Farruggia, P.B. Savage, J. Am. Chem. Soc. 128 (2006) 344–350.
[62] M. Mameli, M.C. Aragoni, V. Lippolis, Inorg. Chem. 48 (2009) 9236–9249.
[63] P. Thordarson, Chem. Soc. Rev. 40 (2011) 1305–1323.